Hindawi
Advances in Civil Engineering
Volume 2022, Article ID 1868617, 13 pages
https://doi.org/10.1155/2022/1868617

Research Article

Performance of Steel Fiber-Reinforced Concrete Pier under Impact Load

Melaknesh Dessalegn [1] **and Temesgen Wondimu** [2]

[1]*Civil Engineering, Wollo University, Kombolcha Institute of Technology, Kombolcha, Ethiopia*
[2]*Civil Engineering, Addis Ababa Science and Technology University, Addis Ababa, Ethiopia*

Correspondence should be addressed to Temesgen Wondimu; temesgen.wondimu@aastu.edu.et

Received 6 February 2022; Revised 20 March 2022; Accepted 28 April 2022; Published 28 May 2022

Academic Editor: Maria Teresa De Risi

Vehicular impact on bridge piers is one of the leading causes of bridge failure. Due to the increase in vehicle-pier collisions, many researchers have studied the performance of RC bridge piers under vehicle collisions. Adding steel fiber is an alternative way to improve the impact resistance of concrete structures and enhance their capacity for energy absorption. However, a study on the performance of piers with steel fiber-reinforced concrete under impact load is limited. This study examines the performance of steel fiber-reinforced concrete (SFRC) bridge piers subjected to impact loading. To study the impact behavior of SFRC piers, a numerical model of bridge piers with impact mass was developed by LS-DYNA. The reliability of the numerical analysis was validated. To investigate the effects of impact mass, impact velocity, the volume of steel fiber, concrete grade, and percentage of longitudinal reinforcement on the impact behaviors of piers and the impact forces, parametric studies were carried out. The finite element analysis revealed that the addition of steel fiber resists lateral deformation and significantly affected the failure modes of bridge piers under impact loading. Moreover, the deformation of the impacted piers and the impact force is mainly affected by the addition of steel fiber, impact energy, and percentage of longitudinal reinforcement and is not sensitive to concrete strength.

1. Introduction

Vehicle collision of bridge piers is one of the leading causes of bridge failure. Due to the increase in vehicle-pier collisions in the past few years, there has been an increase in the number of studies on bridge pier collisions using finite element simulations [1, 2]. These collisions have caused severe damage to bridge structures, such as bridge collapse (see Figure 1) and pier fracture, while other accidents have caused slight damage to piers, such as cracking of concrete (see Figure 2) at the impact location [4, 5]. Therefore, it is necessary to improve the impact resistance of bridge piers to give bridges a long service life and to study the requirements and damage modes to concrete piers.

The addition of fibers is an alternative technique to enhance the impact resistance of bridge piers. Fiber-reinforced concrete (FRC) is a cement-based composite reinforced with discrete fibers that are usually randomly distributed. Fibers are added to the concrete mixture to bridge discrete cracks, thus increasing the control of the fracture process, also increasing the fracture energy, and providing more ductile behavior [6]. Fiber-reinforced concrete (FRC) has been demonstrated to exhibit superior resistance to high strain rate loads compared to conventional concrete, in addition to better control of plastic shrinkage and crack expansion. Therefore, fiber-reinforced concrete is more typically employed to resist impact or blast loads in designed structures [7, 8].

Steel fiber-reinforced concrete is a composite material consisting of a cement matrix and steel fibers as discontinuous reinforcement that can be efficiently used in structural applications. This material has good ductile properties and improves energy dissipation by increasing tensile strength and impact toughness even when exposed to

Figure 1: Bridge collapse [3].

Figure 2: Concrete cracking [3].

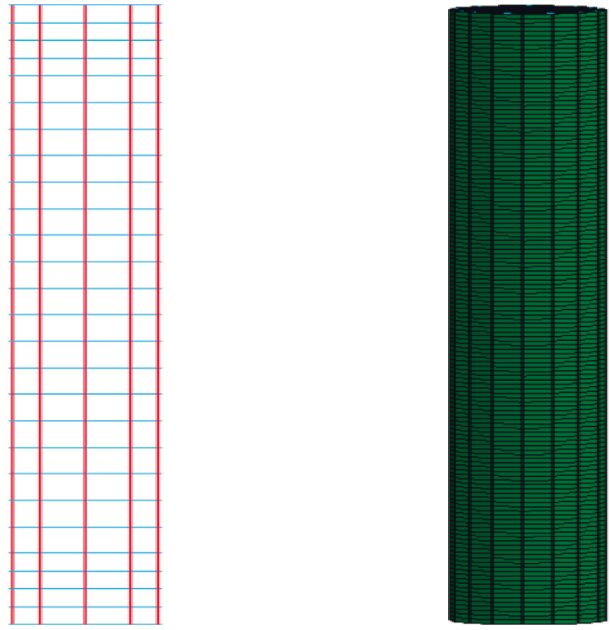

Figure 3: Cross-sectional and reinforcement layout model of a pier in LS-DYNA.

fairly high temperatures. Steel fibers embedded in concrete are less susceptible to corrosion. The increased toughness minimizes or prevents cracks due to relative humidity, temperature changes, etc. Its inclusion also increases the resistance to dynamic loads [9–12].

The energy absorption capabilities of concrete can be enhanced due to the presence of fibers [13]. According to Ulzurrun et al. [14], the fiber-reinforced concrete beams have been shown more than three times higher energy absorption capacity than normal concrete for the same tested configuration. The addition of steel fibers allowed the concrete to exhibit more ductility and enhanced post-cracking behavior compared to the completely fragile behavior exhibited by plain concrete.

Numerical and experimental studies of RC beams with steel fibers subjected to impact loading were investigated by Jin et al. [10]. They investigated the dynamic mechanical behavior of SFRC beams under free-falling drop-weight impacts by testing 12 simply supported SFRC beams with varying stirrup ratios (0%, 0.253%, and 0.502%) and different volume fractions of steel fibers (0%, 1%, 2%, and 3%). The findings indicate that the impact resistance of SFRC beams, such as crack pattern, ductility, energy dissipation capacity, and deformation recovery, can be improved by the inclusion of steel fibers and stirrups.

The addition of fibers has a significant effect on the ductility of the brittle damage mechanism, bridging the tensile stresses even at wide crack openings through the pull-out mechanism. These fibers effectively limit the extension of microcracks that are consistently found in concrete. Steel fibers in concrete reduce the stress concentration near microcracks by the fibers and bridge the cracks and transmit part of the load across the cracks [14–18]. The strengthening mechanism is intimately associated with the mixing ratio and micro/mesostructure of the SFRC, the geometric features, and the mechanical properties of the steel fibers. Thus, for impulsive action, preventing fragile failure, it seems that FRC is a suitable substitute for conventional concrete [10, 14]. Overall, most of these studies are concerned with the investigation of the behavior of SFRC beams under impact load. Nevertheless, investigation of the behavior and the performance of steel fiber-reinforced concrete piers under impact loading are limited. Hence, this study was conducted to examine the performance of SFRC piers under impact loading. In addition, it also studied the parameters that can cause severe damage to bridge piers and the behavior and failure patterns of impacted piers. The pier model was validated by comparing numerical displacements, impact forces, and crack patterns with experimental results of the drop hammer impact test on SFRC beams. In this study, the experiments conducted by Jin et al. [10] were used for validating the finite element controls and material properties for the pier simulations under impact load. Based on the validated numerical, a parametric study was conducted to examine the influence of impact parameters and the behavior of reinforced concrete piers during vehicle collisions. The study parameters include impact mass, impact velocity,

Table 1: Design values of a reinforced concrete pier.

Effective height (m)	Diameter (mm)	Compressive strength of concrete (MPa)	Longitudinal reinforcement size	Stirrup size	Reinforcement ratio (%)
3.5	400	30	$10\phi 12$ mm	$\Phi 8^*$mm	0.9

Table 2: Physical properties of steel fiber.

Length (mm)	Diameter (mm)	Aspect ratio	Tensile strength (MPa)	Density (g/cm^3)	Shape
30	0.6	50	1100	7.8	Hooked-end

Table 3: Material properties.

Parameter	*MAT_CONCRETE_ DAMAGE_REL3	*MAT_PIECEWISE_LINEAR_ PLASTICITY	
	Concrete	Longitudinal bar	Stirrup
Yield strength (MPa)	—	400	300
Density (kg/m^3)	2500	7850	7850
Elastic modulus (GPa)	—	200	200
Poisson's ratio	0.2	0.3	0.3
Compressive strength (MPa)	30	—	—

the volume of steel fibers, concrete grade, and percentage of longitudinal reinforcement.

2. Numerical Model

2.1. Pier Model. In this study, the bridge pier details were taken from Liu et al. [19]. The finite element pier model is shown in Figure 3, and design values are listed in Table 1.

To study the impact behavior of RC and SFRC bridge pier, different FE pier models were analyzed. The effective height of the pier is 3.5 m. The cross-sectional diameter of the pier is 0.4 m. As shown in Table 1, all specimens were modeled with the same cross-sectional area and effective height. The physical properties of steel fiber are shown in Table 2.

Concrete and steel were modeled by solid and beam elements, respectively. The mesh size of each element is 25 mm × 25 mm. The behavior of the concrete beam was simulated using Karagozian and Case (K&C) concrete (KCC) material model * is MAT_072R3 (CONCRTE_DAMAGE_REL3) that has been implemented in LS-DYNA. The KCC model includes material parameter generation based on the unconfined compressive strength of concrete. In addition, this model allows the user to specify a complete set of model parameters from the material test data. The concrete damage model is a three-invariant model that uses three shear failure surfaces and includes strain rate and damage effects. It handles the volumetric and deviatoric responses separately, as often done by explicit codes. This material model is a plasticity-based formulation with three independent surfaces, which change shape based on pressure [20–22]. The values shown in Table 3 were adopted in this study.

The plasticity model for concrete is represented in principal stress space. The general features of the failure surface are described by its cross-sectional shape in the deviatoric plane and its trace on the meridian plane. The constitutive model is defined in terms of stress invariants [23, 24]. The three strength surfaces allow the calculation of the strain hardening and softening behavior according to the η-λ relationship, as shown in Figure 4. The function η (λ) increases up to unity at $\lambda = \lambda$m during the shift of the current surface from the yield surface to the maximum surface, which corresponds to the hardening stage. Subsequently, η gradually decreases to zero as the current surface moves from the maximum strength surface to the residual strength surface. This state represents the softening behavior of the material [23, 25]. However, based on automatically generated parameters, numerical results may be inappropriate for simulating the response of SFRC structures because the material properties of SFRC change with the addition of steel fibers. The relation between the parameter η and the damage parameter λ or the damage evolution parameters b1 and b2 in the K&C model should be modified. And the strength surfaces should be modified based on several experimental triaxial compressive tests on SFRC specimens.

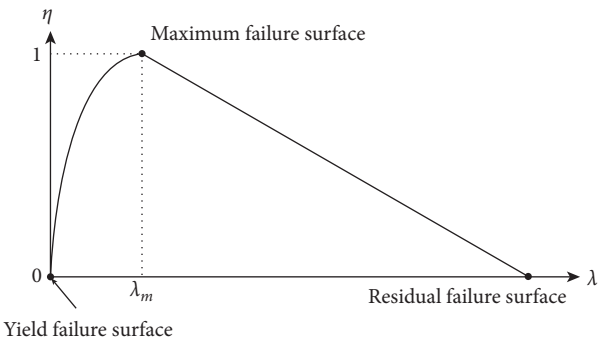

Figure 4: Diagram of the function η (λ) [23].

(i) Maximum strength surface:

$$\Delta\sigma = \begin{cases} \alpha 3\dfrac{p}{(\alpha_1 + \alpha_2 p)}, & \text{for} p \geq \dfrac{f_c}{3}, \\ (p + f_t), & \text{for}\left\{0 \leq p\dfrac{f_c}{3}\right\} or \left\{\lambda \leq \lambda_3 \text{and} -T \leq p \leq \dfrac{f_c}{3}\right\}, \\ 2\psi, & \\ 3\left(\left(\dfrac{p}{\eta + f_t}\right)\right), & \text{for} p \leq 0 \text{and} \lambda > \lambda_m, \end{cases} \tag{1}$$

$$\alpha_0 = 0.2956 f_c, \alpha_1 = 0.4463 an\, d\alpha_2 = \frac{0.8080}{fc}. \tag{2}$$

(ii) Yield strength surface:

$$\Delta\sigma_y = \begin{cases} \alpha_{0y} + \dfrac{p}{\left(\alpha_{1y} + \alpha_{2y} p\right)}, & \text{for} p \geq \dfrac{f_{yc}}{3}, \\ 1.35 f_t + 3p\left(1 - 1.35\dfrac{f_t}{f_{yc}}\right), & \text{for} 0 \leq p \leq \dfrac{f_{yc}}{3}, \\ 1.35\left(p + f_t\right), & \text{for} p \leq 0, \end{cases} \tag{3}$$

$$\begin{aligned} \alpha_{0y} &= 0.2232 f_c, \\ \alpha_{1y} &= 0.625\alpha_{2y} = \frac{0.2575}{f_c}. \end{aligned} \tag{4}$$

(iii) Residual strength surface:

$$\Delta_{\sigma f} = \frac{p}{\alpha_{1f} + \alpha_{2f} p}, \tag{5}$$

$$\begin{aligned} \alpha_{0f} &= 0, a_{1f} = 0.4417, \\ \alpha_{2f} &= \frac{0.1183}{f_c}. \end{aligned} \tag{6}$$

According to Lee et al. [23], the modified equations for the strength surfaces are

$$\begin{aligned} \alpha_0 &= 0.34339 f_c, \\ \alpha_1 &= 0.40967, \\ \alpha_2 &= \frac{0.05554}{fc}, \end{aligned} \tag{7}$$

$$\begin{aligned} \alpha_{0y} &= 0.28606 f_c, \\ \alpha_{1y} &= 0.79045, \\ \alpha_{2y} &= \frac{0.14515}{fc}, \end{aligned} \tag{8}$$

$$\begin{aligned} \alpha_{0f} &= 0, \\ \alpha_{1f} &= 0.4669, \\ \alpha_{2f} &= \frac{0.05421}{f_c}. \end{aligned} \tag{9}$$

The correlation between η and λ can be formulated as

$$\eta(\lambda) = \begin{cases} \alpha\dfrac{\lambda}{\lambda m} + (3 - 2\alpha)\left(\dfrac{\lambda}{\lambda m}\right)^2 + (\alpha - 2)\left(\dfrac{\lambda}{\lambda m}\right)^3, & \lambda < \lambda_m, \\ \dfrac{(\lambda/\lambda m)}{\alpha c\,(\lambda/\lambda m - 1)^{\alpha d} + \lambda/\lambda m}, & \lambda \geq \lambda_m, \end{cases} \tag{10}$$

where α, αc, and αd are the parameters that affect the shape of the hardening and softening regions of the stress-strain relationship, respectively. The parameter λm corresponding to $\eta = 1$ is associated with the peak strain. The parameters α and αc affect the overall shape of the hardening and softening regions, respectively, and αd affects the residual part of the softening region. Since the addition of steel fibers had almost no effect on the shape of the hardened part, the value of α was fixed at 2. Material Model 03 (MA_PLASTIC_KINEMATIC) uses for modeling steel reinforcement. This material model is capable of isotropic and kinematic hardening plasticity including the strain effect. As compared to other models for steel, it is a relatively simple bilinear model, but it is very cost-effective in computational resources [1, 26].

2.2. Contact Type. In this study, the AUTOMATIC SURFACE-TO-SURFACE contact algorithm in LS- DYNA was defined. To have a realistic simulation under body interaction, static friction coefficients (0.1) and dynamic friction coefficients (0.1) between the SFRC surface of the beam and the drop hammer were applied to the entire bodies.

2.3. Model Validation. To ensure that it is accurate that the finite element analysis of the model represents what is depicted and idealizes the real behavior of the specimen tested, validation is first conducted. Since experimental data on vehicle-pier collisions are very limited, an experiment representing a similar impact phenomenon is used for validation. The numerical model was validated by matching impact force and displacement with experimental results and by comparing the crack patterns with the published data of the drop hammer impact test on SFRC beams [10]. There were twelve SFRC 3-point bending beams arranged with different volume fractions of steel fibers (0%, 1%, 2%, and 3%) and stirrup ratios (0%, 0.253%, and 0.502%) for the laboratory experiments performed by Jin et al. [10]. The SFRC beams had dimensions of 2800 mm × 200 mm × 400 mm (length, width, and height) and a cover thickness of 30 mm. The weight of the hammer applied on the SFRC beam is 393 kg with a velocity of 7.2 m/s. The drop hammer impact test setup and detailed reinforcement layout are depicted in Figures 5 and 6, respectively.

In this study, four types of beams were modeled, each with a different ratio of steel fibers. The first (B-0- 25), second (B-1-25), third (B-2-25), and fourth (B-3-25) beams consisted of volume fraction of steel fibers, ρfiber of 0%, 1%, 2%, and 3%, respectively, and stirrup ratio, ρsv of 0.253%.

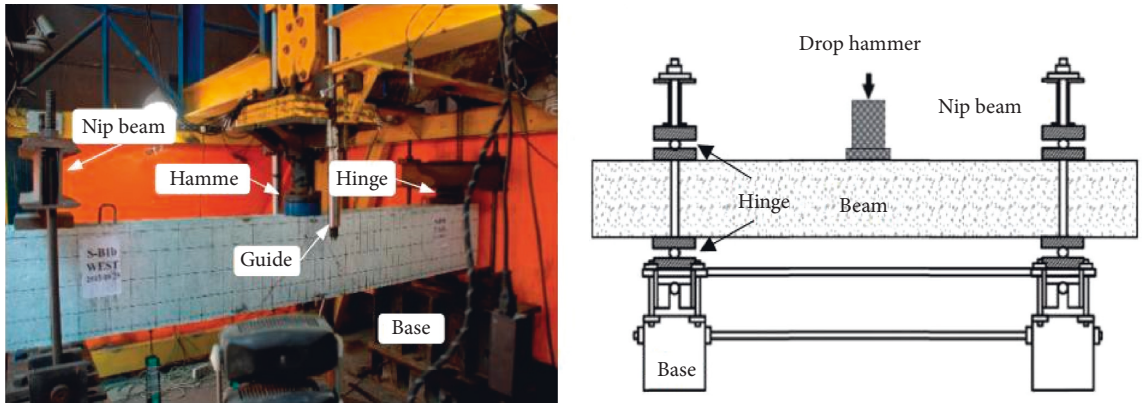

Figure 5: The drop hammer impact test setup [10].

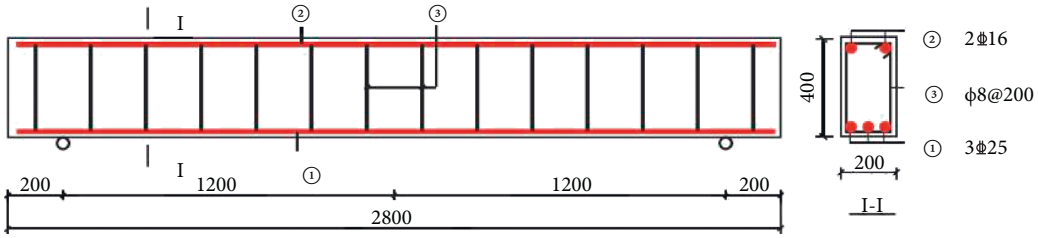

B-0-25/B-1-25/B-2-25/B-3-25

Figure 6: Dimensions and reinforcement layout of RC and SFRC beams [10].

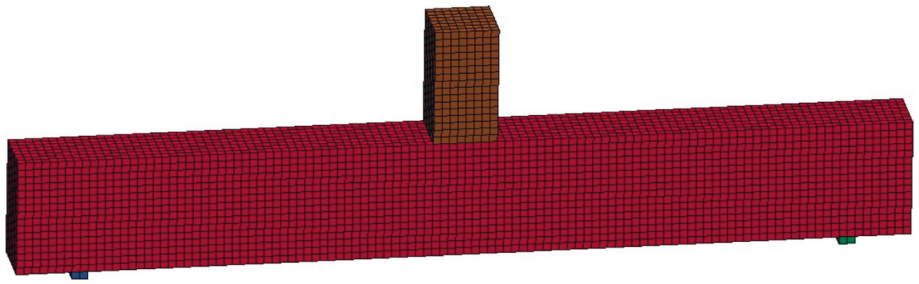

Figure 7: Finite element model of reinforced concrete beam and drop hammer.

The numerical model of the impact test was developed in LS-DYAN and is shown in Figure 7. Table 3 shows the properties of concrete and reinforcement bar used in LS-DYNA. Concrete and steel fiber were modeled by CONCRTE_DAMAGE_REL3. The reinforcement bar was modeled by MAT_PLASTIC_KINEMATIC. The contact type between drop hammer and beam was AUTOMATIC SURFACE TO SURFACE.

The comparison of the midspan deflection time-history of the beams obtained by the LS-DYNA and the experimental test results of the beam B-0-25 is shown in Figure 8. As can be observed from Figure 8(a), the midspan deflection of numerical results agrees well with the experimental measurements. The maximum displacement of the impact test and numerical result is 31.4 mm and 30.2 mm, respectively; the difference is 3.8%. As it is depicted to the midspan deflection of beams B-1-25, B-2-25, and B-3-25, the numerical results are in good agreement with the experimental measurements before the peak value of the midspan deflection time-history, while the post-peak value of the vibration has not been deflected in the simulations. Nevertheless, it can still be said that the numerical simulations adequately capture the responses of steel fiber-reinforced concrete beams under impact loading.

The comparison of the impact force-time-history between numerical simulation and experimental measurement of beams B-0-25, B-1-25, B-2-25, and B-3-25 is shown in Figure 9. It is observed that time-histories of impact forces of these beams are accurately predicted by numerical simulation with the experimental result.

2.4. Hourglass Control of the Numerical Result. The time-history curves of various energies in a B-1-25 impact simulation are shown in Figure 10. Here, hourglass energy is very low, around 5% of total energy (<10%). Therefore, the

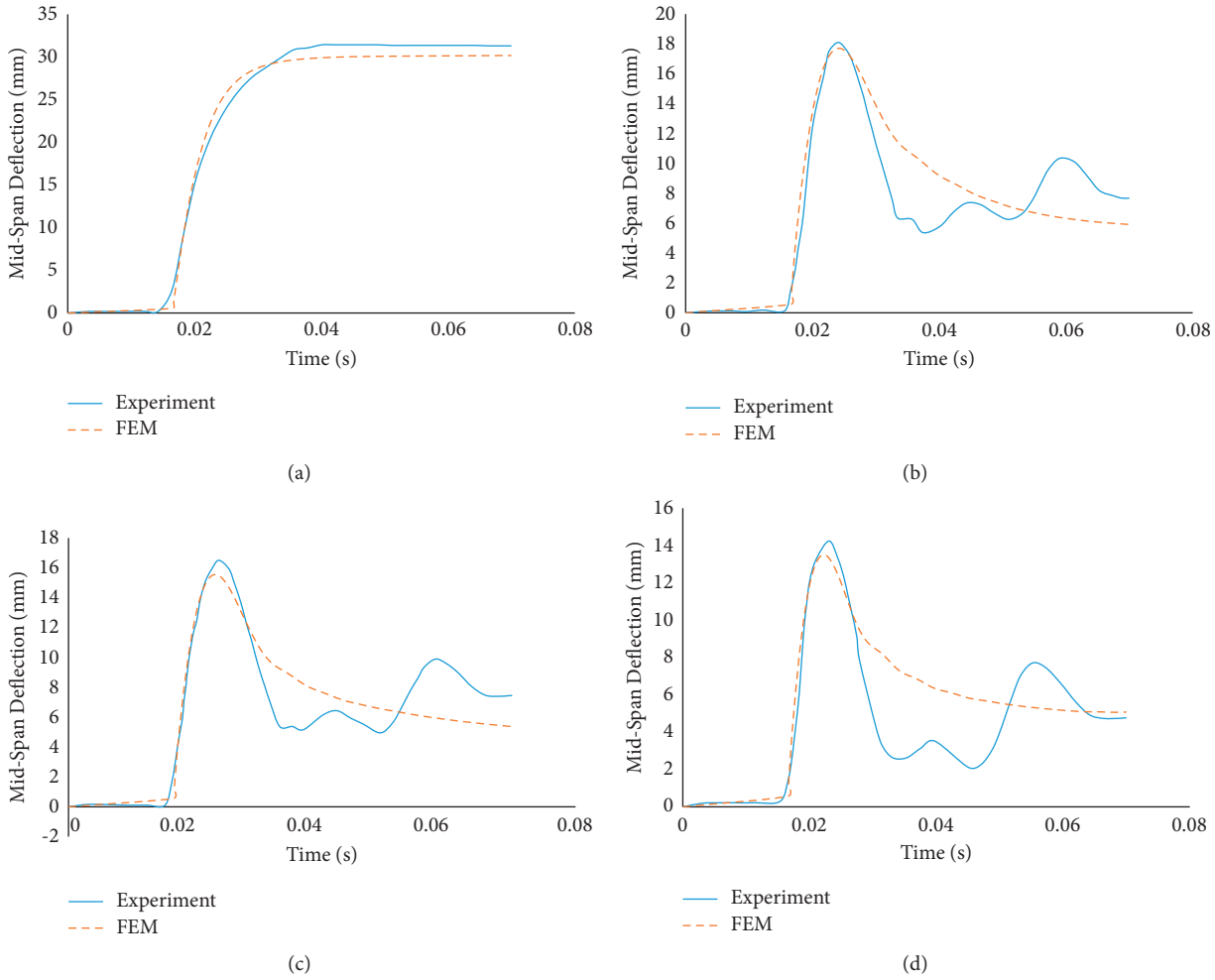

Figure 8: Comparison between the midspan deflections of the beam obtained by numerical simulation and experimental observation: (a) B-0-25, (b) B-1-25, (c) B-2-25, and (d) B-3-25.

low amount of hourglass energy relative to the total energy in impact simulation demonstrates the acceptance of analysis results.

3. Numerical Analysis and Parametric Studies

Once the numerical model is validated, a parametric study was conducted to examine the influence of impact parameters and the behavior of reinforced concrete piers subjected to impact load. These parameters include impact mass, impact velocity, the volume of steel fibers, concrete grade, and percentage of longitudinal reinforcement. The summarized information of the studied parameters is presented in Table 4.

3.1. Effect of Impact Mass. To study the effect of impact mass on the impact forces, displacements, and impact behaviors of piers under impact load, three finite element pier models were analyzed under impact load by assuming three impact masses (3.5 tonnes, 10 tonnes, and 30 tonnes). In this FE analysis, the velocity of the impactor and volume of fiber content was 60 km/hr and 0%, respectively. And the concrete grade used is 30 MPa with the percentage of longitudinal reinforcement, 0.9%. The analysis results in terms of displacement and impact force time-history curves corresponding to different impact masses are shown in Figures 11 and 12, respectively. The displacement time-history curves indicate that the maximum displacement increases as impact mass increases. The maximum displacement of impact masses 3.5 tonne and 30 tonne had decreased by 9.2% and increased by 1.27%, respectively, as compared to the control specimen (10 tonne) when other parameters were kept constant. In addition, the impact force was found to have a proportional relationship with impact mass, as shown in Figure 12. The peak impact force of impact masses of 3.5 tonne and 30 tonne had decreased by 0.37% and increased by 1.45%, respectively, as compared to the control specimen (10 tonne).

3.2. Effect of Impact Velocity. The impact velocities used in this study are 30, 60, and 90 km/hr to investigate their effects on the behavior of bridge piers under impact load. In this FE analysis, the mass of the impactor and volume of fiber content was 10tonne and 0%, respectively. In a finite element

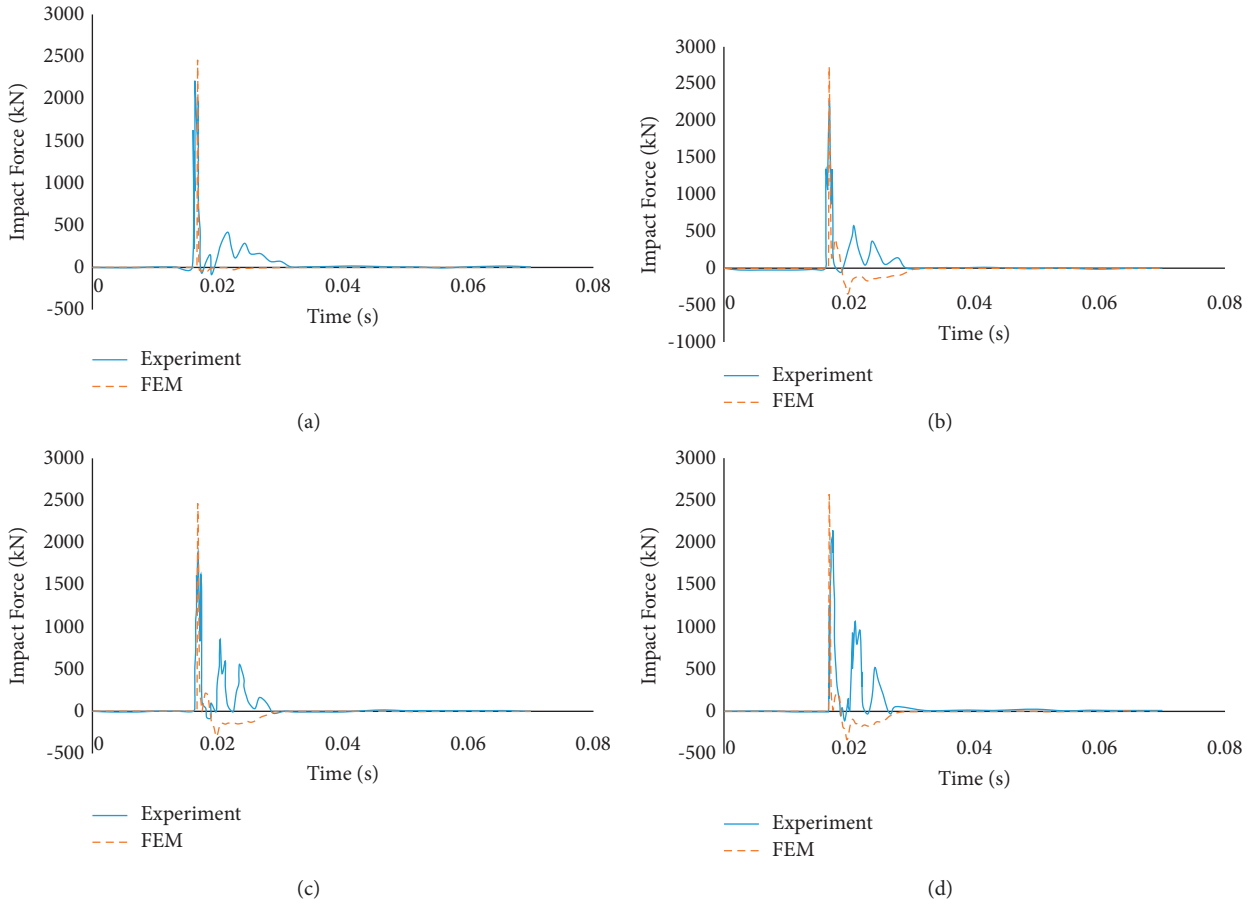

Figure 9: Comparison between the impact forces of the beams obtained by numerical simulation and experimental observation: (a) B-0-25, (b) B-1-25, (c) B-2-25, and (d) B-3-25.

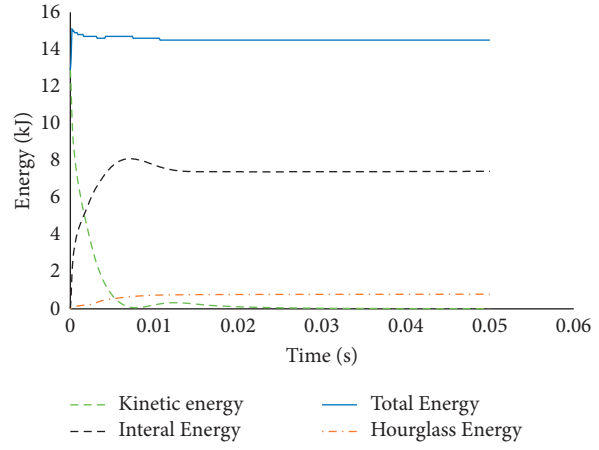

Figure 10: Development of various energies.

Table 4: Study parameter details.

Impact mass, M (tonne)	Impact velocity, V (km/hr)	Volume of steel fiber, SF (%)	Concrete grade, CG (MPa)	Percentage of longitudinal reinforcement, LR (%)
$M1 = 3.5$	$V1 = 30$	SF0 = 0%	CG1 = 30	LR1 = 0.9
$M2 = 10$	$V2 = 60$	SF1 = 1%	CG2 = 60	LR2 = 1.6
$M3 = 30$	$V3 = 90$	SF2 = 2%	CG3 = 90	LR3 = 3.6

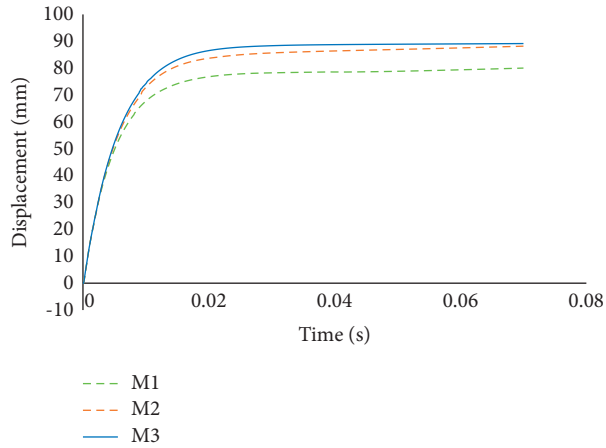

Figure 11: Displacement time-history curves for different impact masses.

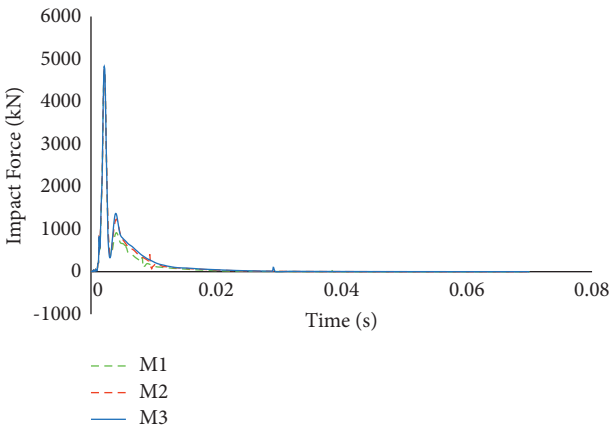

Figure 12: Impact force time-history curves for different impact masses.

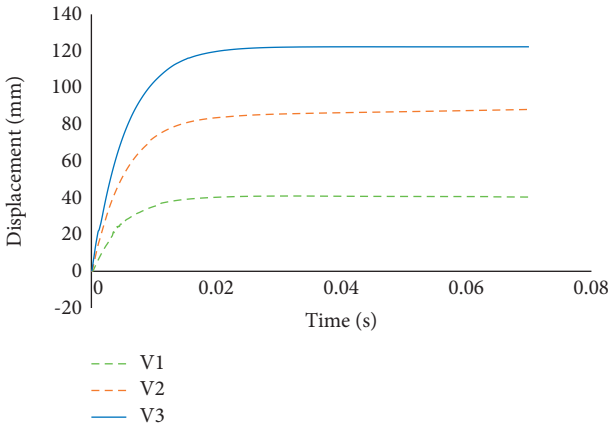

Figure 13: Displacement time-history curves for different impact velocities.

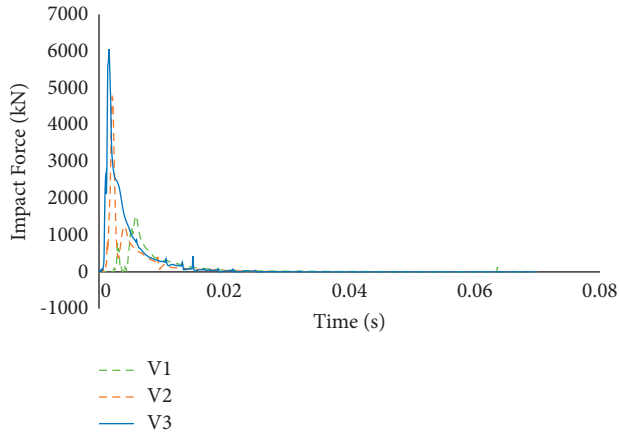

Figure 14: Impact force time-history curves for different impact velocities.

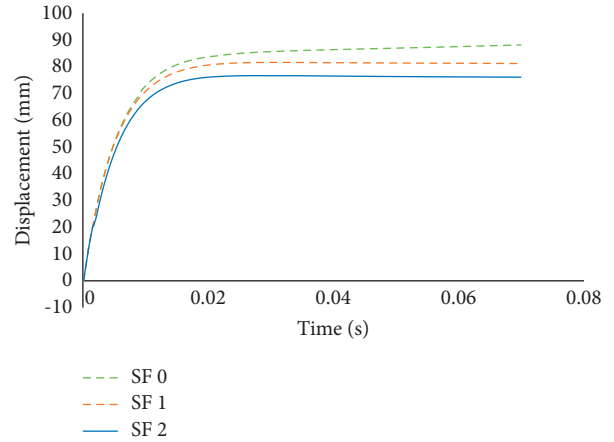

Figure 15: Displacement time-history curves for different volumes of steel fiber.

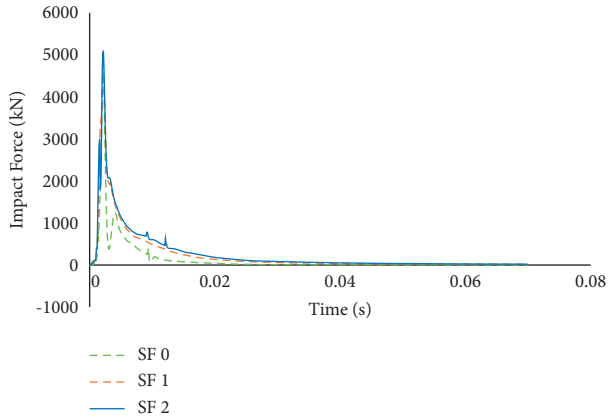

Figure 16: Impact force time-history curves for different volumes of steel fiber.

analysis result, the influence of the difference in impact velocity on maximum displacement and peak impact force of RC piers was investigated. The displacement time-history curves for different impact velocities are shown in Figure 13.

As it can be observed, when impact velocity increases, the displacement increases. As impact velocity increases from 30 km/h to 60 km/h, the maximum displacement increases by 53.4%. The maximum displacement of the impacted pier

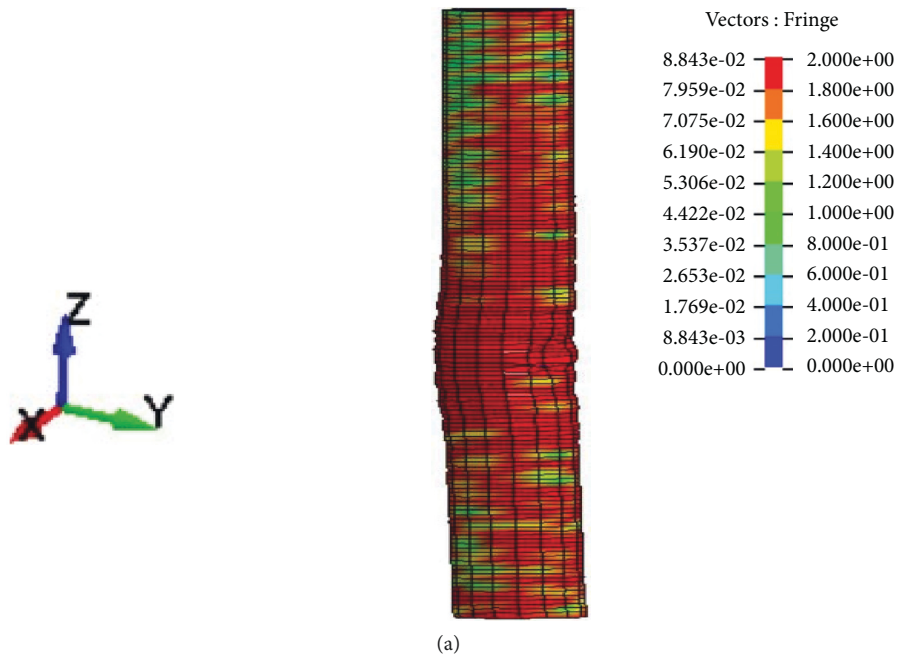

(a)

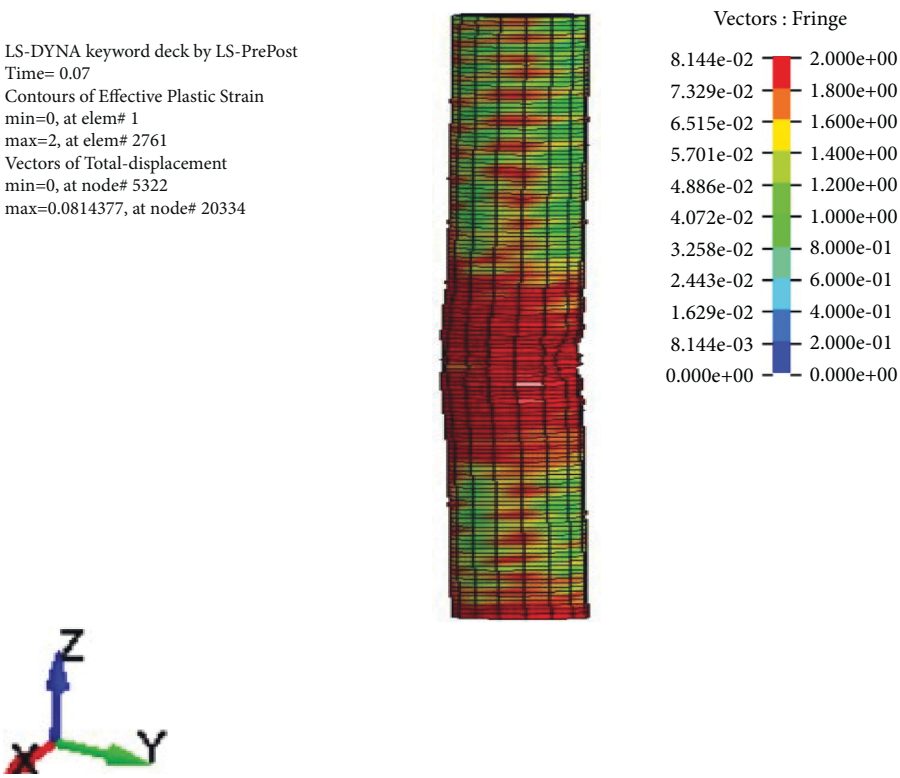

(b)

Figure 17: Continued.

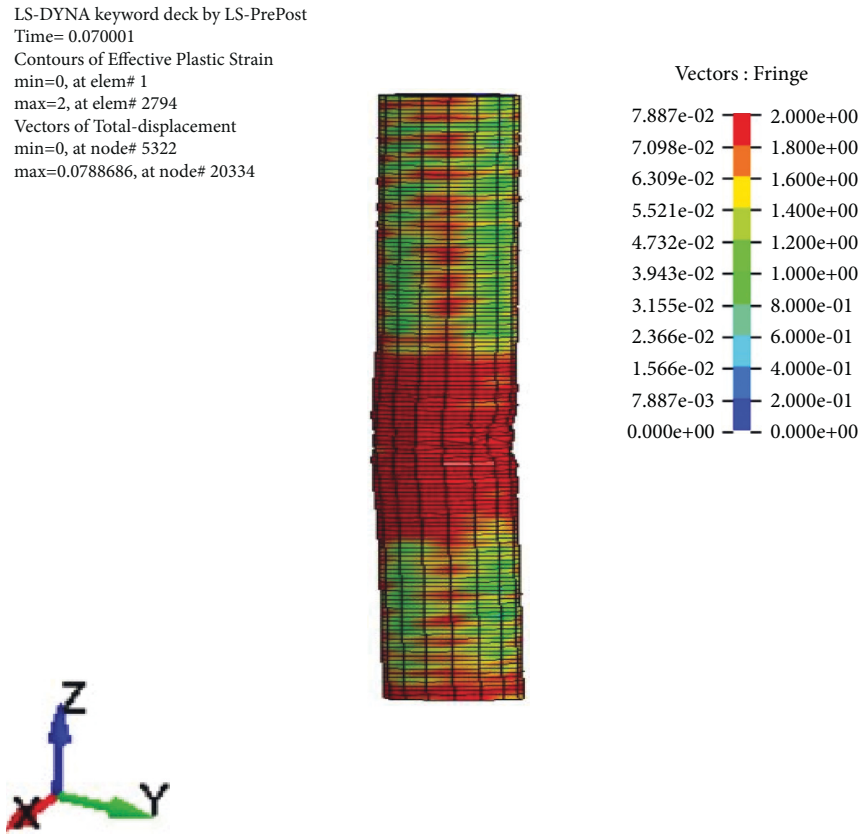

and (c)

Figure 17: Concrete damage modes for different volumes of steel fiber. (a) SF0 = 0% steel fiber, (b) SF1 = 1% steel fiber, and (c) SF2 = 2% steel fiber.

increased by 38.7% when the impact velocity increases from 60 km/hr to 90 km/hr. As shown in Figure 14, the time-history curves of the impact forces were correlated to varying impact velocities. One can observe that the maximum impact force increases when there is an increase in the impact velocity. When the impact velocity increases from 30 km/h to 60 km/h, the peak impact force increases by 68%, and when the impact velocity increases from 60 km/h to 90 km/h, the peak impact force increases by 27.4%.

The main factor for this result lies in the impact energy. An increase in impact velocity leads to higher impact energy, resulting in a bigger maximum impact force. As demonstrated in the figure, impact velocity also affects impact duration. The higher impact velocity also resulted in a relatively longer impact duration because of the higher deformation of the bridge pier due to the absorption of higher impact energy.

3.3. Effect of Volume of Steel Fiber. In this study, an investigation of the effect of the volume of steel fiber on the behavior of bridge piers under impact load is conducted with different volumes of steel fibers (0%, 1%, and 2%) using finite element simulation. In this FEM model, the mass and velocity of the impactor were 10 tonne and 60 km/hr, respectively. And pier with 30 MPa and 0.9% longitudinal reinforcement is used. In a finite element analysis result, the influence of the difference in the volume of steel fiber on maximum displacement, peak impact force, and failure patterns of bridge piers was investigated. The time-history curves of maximum displacement of a pier for different volume steel fibers are illustrated in Figure 15. When a 1% volume of steel fiber is added, the maximum displacement decreases by 7.4% compared to the control specimen (0%) when other parameters were kept constant. When the volume of steel fiber increases to 2%, the maximum displacement decreases by 13.04% compared to the control specimen (0%) when other parameters were kept constant. The time-history curves of the impact force of a pier for different volumes of steel fibers are shown in Figure 16. When a 1% volume of steel fiber is added, the peak impact force increases by 9.7% compared to the control specimen (0%) when other parameters were kept constant. When the volume of steel fiber increases to 2%, the peak impact force increases by 6.7% compared to the control specimen (0%) when other parameters were kept constant.

The failure patterns of piers for different volumes of steel fibers are shown in Figure 17. When the volume of steel fiber is 0%, the bridge pier experienced local damage and lateral deformation at the impact location. As the volume of steel fiber increases to 1% and 2%, local damage occurred at the impacted area. It can be observed that the lateral deformation of piers decreases as the volume of steel fiber increases.

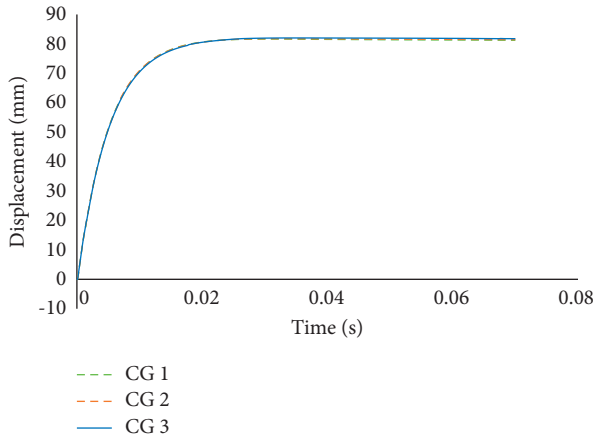

Figure 18: Displacement time-history curves for different concrete grades with steel fiber.

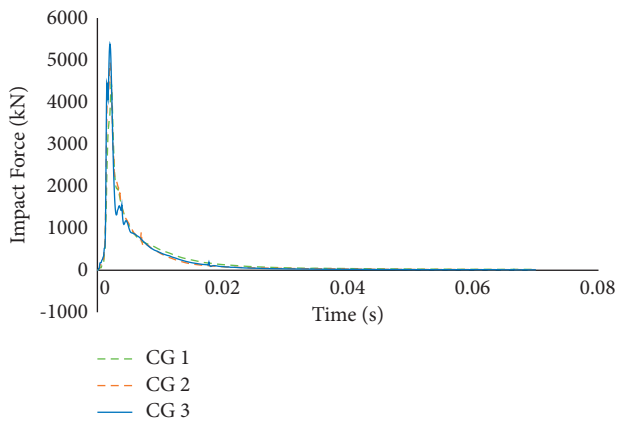

Figure 19: Impact force time-history curves for different concrete grades with steel fiber.

3.4. Effect of Concrete Grade. To investigate the effect of concrete grade on the impact behavior of displacement and impact force of bridge piers, three FE pier models with concrete compressive strength of 30, 60, and 90 MPa with steel fiber were analyzed. In these models, the mass and velocity of the impactor are 10 tonnes and 60 km/hr, respectively. And the percentage of longitudinal reinforcement was 0.9%. To investigate the effect of the concrete grade on the impact behavior of the pier, 1% steel fiber is used. The displacement time-history curves for different grades of concrete with steel fiber are shown in Figure 18. As shown, all the peak displacements are about 82 mm, which indicates that the impact resistance of the bridge piers is almost insensitive to the concrete strength. This is because the deformation is mainly governed by the pier stiffness and the impact energy, whereas the stiffness of the pier is almost not influenced by the strength of the concrete. Hence, the effect of concrete strength on the maximum displacement is small when the impact energy and the geometry of the bridge pier remain constant. The impact force time-history curves of different strengths of concrete with steel fibers are shown in Figure 19. As it can be observed, the peak impact force of a pier increased by 11.4% when the concrete strength with steel fiber increased from 30 MPa (control specimen) to 60 MPa. And the peak impact force of a pier increased by 21.4% when the concrete strength with steel fiber increased from 30 MPa to 90 MPa.

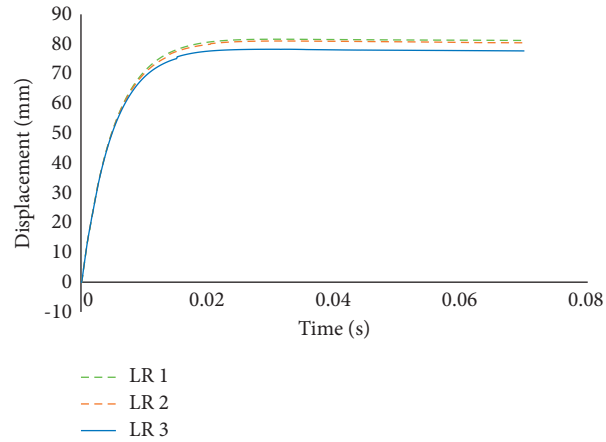

Figure 20: Displacement time-history curves for different percentages of longitudinal reinforcement with steel fiber.

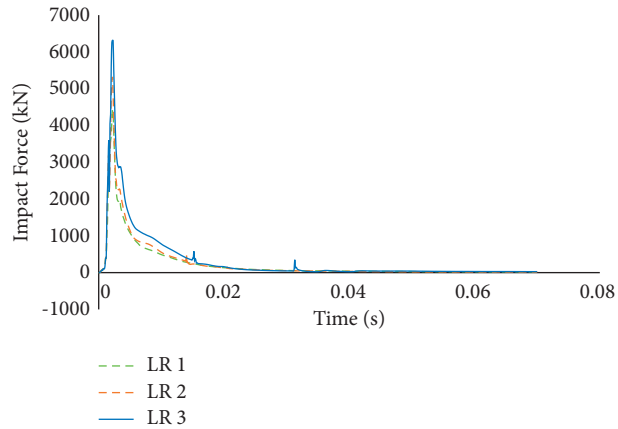

Figure 21: Impact force time-history curves for different percentages of longitudinal reinforcement with steel fiber.

3.5. Effect of the Percentage of Longitudinal Reinforcement. The finite element model of a pier with the percentage of longitudinal reinforcement of 0.9%, 1.6%, and 3.6% with steel fiber was analyzed to determine their effects on maximum displacement and impact force of a pier under impact load. In these models, the mass and velocity of the impactor are 10 tonnes and 60 km/hr, respectively. The compressive strength of the concrete pier was 30 MPa. To investigate the effect of the percentage of longitudinal reinforcement on the impact behavior of the pier, 1% steel fiber is used. The displacement time-history curves corresponding to different percentages of longitudinal reinforcement with steel fiber are depicted in Figure 20. As shown, the peak displacement of piers with 0.9% and 1.6% percentage of longitudinal reinforcement is similar (81 mm), and 78 mm when the percentage of longitudinal reinforcement is 3.6% with steel fiber.

This indicates that the collision resistance of piers with steel fiber is almost insensitive to the percentage of longitudinal reinforcement. This is because the deformation is mainly controlled by impact energy. The impact force time-history curves of different percentages of longitudinal reinforcement with steel fibers are shown in Figure 21. As it can be observed, the peak impact force of a pier increased by 20.1% when the percentage of longitudinal reinforcement with steel fiber increased from 0.9% (control specimen) to 1.6%. And the peak impact force of a pier increased by 42.5% when the percentage of longitudinal reinforcement with steel fiber increased from 0.9% to 3.6%.

4. Conclusions

This study has investigated the performance of RC and SFRC bridge piers under impact load. In this investigation, a detailed description of finite element modeling of steel fiber-reinforced concrete piers under impact load using LS-DYNA was presented and validated using a nonlinear material constitutive method that considers the effect of strain rate. Depending on the validated numerical model, a parametric study was conducted to examine the effects of impact mass, impact velocity, the volume of steel fiber, concrete grade, and percentage of longitudinal reinforcement on the pier's behavior. Analysis of the relationship among the failure modes of piers was also performed. The following points are the main conclusions drawn from the findings of this research:

(i) Finite element analysis results indicated that the impact response of SFRC beams subjected to impact loadings generated from numerical analysis describes a good agreement with the experimental test conducted previously. This demonstrates the rationality and accuracy of the finite element model used in this investigation to analyze the impact response of the SFRC piers. However, there are some differences in the displacement time-history curves of the SFRC beam specimens after the peak value. Nevertheless, it can be said that the FE model in this research reveals the impact response of the SFRC piers.

(ii) The deformation of the impacted piers and the impact force are principally in control of impact energy. As impact velocity increases from 30 km/h to 60 km/h and 90 km/hr, the maximum displacement increases by 53.4% and 38.7%, respectively. When the impact velocity increases from 30 km/hr to 60 km/hr and 90 km/hr, the peak impact force increases by 68.0% and 27.4%, respectively. In addition, the maximum displacement of impact masses of 3.5 tonne and 30 tonne had decreased by 9.2% and increased by 1.27%, respectively, as compared to the control specimen.

(iii) The deformation is not sensitive to concrete strength. And the peak impact force of a pier increased by 20.1% and 42.5% when the percentage of longitudinal reinforcement with steel fiber is 1.6% and 3.6%, respectively. Therefore, collision resistance of piers is improved with a higher percentage of longitudinal reinforcement, which can resist large impact forces.

(iv) The addition of steel fibers significantly affected the failure mode of the bridge piers under impact loading. The addition of 1% and 2% volume fraction of steel fiber decreases maximum displacement by 7.4% and 13.04%, respectively. Piers without steel fibers exhibited lateral deformation and localized damage, even though the strength of the concrete in the piers was improved. However, piers with steel fibers exhibited localized damage. Therefore, we can conclude that the addition of steel fibers helps to resist the lateral deformation of the piers under impact loading.

Data Availability

The data used to support the findings of the study can be obtained from the corresponding author upon request.

Conflicts of Interest

The authors declare that there are no known conflicts of interest for the publication of this study.Disclosure

This research was made as partial fulfillment of the requirements for the award of Master of Science in structural engineering.

References

[1] A. K. Agrawal, G. Liu, and S. Alampalli, "Effects of truck impacts on bridge piers," *Adv. Mater. Res*, vol. 639–640, pp. 13–25, 2013.

[2] L. Chen, S. El-Tawil, and Y. Xiao, "Reduced models for simulating collisions between trucks and bridge piers," *Journal of Bridge Engineering*, vol. 21, no. 6, p. 04016020, 2016.

[3] D. Zhou, R. Li, J. Wang, and C. Guo, "Study on impact behavior and impact force of bridge pier subjected to vehicle collision," *Shock and Vibration*, vol. 2017, Article ID 7085392, 12 pages, 2017.

[4] X. Xu, R. Cao, S. El-Tawil, A. K. Agrawal, and W. Wong, "Loading definition and Design of bridge piers impacted by medium-weight trucks," *Journal of Bridge Engineering*, vol. 24, no. 6, p. 04019042, 2019.

[5] K. Agrawal, X. Xu, and Z. Chen, "The City College of New York Department of Civil Engineering," *Bridge-vehicle Impact Assessment*, New York, NY 10031, USA, 2011.

[6] A. Jansson, "Fibres in reinforced concrete structures-analysis, experiments and design," 2008, http://publications.lib.chalmers.se/cpl/record/index.xsql?pubid=68889%5Cnhttp://publications.lib.chalmers.se/public%20ation/68889-fibres-in-reinforced-concrete-structures-analysis-experiments-and-design.

[7] S. Shahidan, M. Abdul Rahim, N. S. Nik Zol, M. A. Azizan, and I. Ismail, "Properties of Steel Fiber Reinforcement Concrete with Different Characteristic of Steel Fiber," *Appl. Mech. Mater*, vol. 773–774, pp. 28–32, 2015.

[8] Z. Xu, H. Hao, and H. N. Li, "Experimental study of dynamic compressive properties of fibre reinforced concrete material with different fibres," *Materials & Design*, vol. 33, no. 1, pp. 42–55, 2012.

[9] H. Aylie, Antonius, and A. W. Okiyarta, "Experimental study of steel-fiber reinforced concrete beams with confinement," *Procedia Engineering*, vol. 125, pp. 1030–1035, 2015.
[10] L. Jin, R. Zhang, G. Dou, J. Xu, and X. Du, "Experimental and numerical study of reinforced concrete beams with steel fibers subjected to impact loading," *International Journal of Damage Mechanics*, vol. 27, no. 7, pp. 1058–1083, 2018.
[11] N. Bedewi, "*Steel fiber reinforced concrete made with fibers extracted from used tyres*," Energy, Master's thesis in Civil Engineering, Addis Ababa University, Addis Ababa, Ethiopia, pp. 1–111, 2009.
[12] F. Germano, *Cyclic Behavior of Steel Fiber Reinforced Concrete*, University of Brescia, Brescia, Italy, 2016.
[13] M. Musmar, "Tensile strength of steel fiber reinforced concrete," *Contemporary Engineering Sciences*, vol. 6, no. 5–8, pp. 225–237, 2013.
[14] G. Ulzurrun and C. Zanuy, "Energy absorption of steel fiber-reinforced concrete beams under impact loads," in *Proceedings of the . 11th fib Int. PhD Symp. Civ. Eng. FIB 2016*, pp. 745–752, Madrid, Spain, 2016.
[15] A. Bazgir and F. Fu, "*The behaviour of steel fibre reinforced concrete material and its effect on impact resistance of slabs*," pp. 1–101, Degree of Master of Philosophy in Structural Engineering at City University, London, UK, 2016.
[16] J. Deluce and F. Vecchio, "Cracking behavior of steel fiber-reinforced concrete members containing conventional reinforcement," *ACI Structural Journal*, vol. 110, no. 3, pp. 481–490, 2013.
[17] Y.-S. Yoon and D. Y. Yoo, "Influence of steel fibers and fiber-reinforced polymers on the impact resistance of one-way concrete slabs," *Journal of Composite Materials*, vol. 48, no. 6, pp. 695–706, 2014.
[18] H. P. Behbahani, B. Nematillahi, A. R. Mohd, and F. C. Lai, "Flexural behavior of steel-fiber-added-RC (SFARC) beams with C30 and C50 classes of concrete | international journal of sustainable construction engineering and technology," *Int. J. Sustain. Constr. Eng. Technol.*, vol. 3, 2012.
[19] L. Liu, Z. H. Zong, and M. Li, "Numerical study of damage modes and assessment of circular RC pier under noncontact explosions," *Journal of Bridge Engineering*, vol. 23, no. 9, 2018.
[20] M. Madurapperuma and K. Niwa, "Concrete Material Models in LS-DYNA for Impact Analysis of Reinforced Concrete Structures," *Appl. Mech. Mater*, vol. 566, pp. 173–178, 2014.
[21] N. Markovich, E. Kochavi, and G. Ben-Dor, "Calibration of a concrete damage material model in LS-dyna for a wide range of concrete strengths," in *Proceedings of the IWSRIB_2009_Haifa*, Haifa, Israel, 2009.
[22] A. J. Sangi, *Reinforced Concrete Structures under Impact Loads*, Heriot-Watt University, United Kingdom, 2011.
[23] M. Lee, H.-G. Kwak, and G.-K. Park, "An improved calibration method of the K&C model for modeling steel-fiber reinforced concrete," *Composite Structures*, vol. 269, p. 114010, 2021.
[24] L. J. Malvar and D. Simons, "Concrete material modeling in explicit computations work," in *Proceedings of the Recent Advances in Computational Structural Dynamics and High Performance Computing*, pp. 1–30, USAE Waterways Experiment Stations, April 1996.
[25] Y. Wu and J. E. Crawford, "Numerical modeling of concrete using a partially associative plasticity model," *Journal of Engineering Mechanics*, vol. 141, no. 12, p. 04015051, 2015.
[26] T. A. Mohammed, D. Ph, A. Parvin, and D. Sc, "Vehicle collision impact response of bridge pier strengthened with composites," vol. 25, no. 1741, pp. 1–9, 2020.